Structural Engineering and Mechanics, *Vol. 74, No. 5 (2020) 711-722*
DOI: https://doi.org/10.12989/sem.2020.74.5.711

Experimental study on vibration serviceability of steel-concrete composite floor

Liang Cao*[1,2], Jiepeng Liu[1,2a] and Y. Frank Chen[1,2a]

[1]*School of Civil Engineering, Chongqing University, Chongqing 400045, China*
[2]*Key Laboratory of New Technology for Construction of Cities in Mountain Area (Chongqing University), Ministry of Education, Chongqing 400045, China*

(Received August 22, 2019, Revised December 25, 2019, Accepted January 23, 2020)

Abstract. In this study, on-site testing was carried out to investigate the vibration serviceability of a composite steel-bar truss slab with steel girder system. Impulse excitations (heel-drop and jumping) and steady-state motion (walking and running) were performed to capture the primary vibration parameters (natural frequency and damping ratio) and distribution of peak acceleration. The composite floor possesses low frequency (<8.3Hz) and damping ratio (<2.47%). Based on experimental, theoretical, and numerical analyses on fundamental natural frequency, the boundary condition of SCSS (i.e., three edges simply supported and one edge clamped) is deemed more comparable substitutive for the investigated composite floor. Walking and running excitations by one person (single excitation) were considered to evaluate the vibration serviceability of the composite floor. The measured acceleration results show a satisfactory vibration perceptibility. For design convenience and safety, a crest factor β_{rp} describing the ratio of peak acceleration to root-mean-square acceleration induced from the walking and running excitations is proposed. The comparisons of the modal parameters determined by walking and running tests reveal the interaction effect between the human excitation and the composite floor.

Keywords: steel-bar truss slab; composite floor; human-structure interaction; vibration serviceability; crest factor

1. Introduction

The existing complexity of large span composite structures (Jrad *et al*. 2018, Wang *et al*. 2017) and people's higher demand of living comfort has resulted in a constant exploration for economically efficient structural forms in structural engineering. The composite steel-bar truss slab with steel girder (Fig. 1) is a modern composite structure consisting of steel girder, steel-bar truss slab, and the reinforced concrete (RC) slab cast in place. The composite steel-bar truss slab with steel girder is an economical form of floor construction as it does not require any formwork. It has been commonly used in China and other places in Asia. Compared with traditional floor structures, the composite steel-bar truss slab with steel girder possesses the following features:

(1) It fully utilizes the advantages of steel and concrete materials;

(2) The steel sheeting serves as the permanent formwork and there is no need of any additional formwork, thus speeding up the construction process;

(3) It has better structural integrity;

(4) It has good seismic resistance (as with traditional composite floors) (Yan and Lu 2015).

As shown in Fig. 1, the steel-bar truss slab consists of reinforcing bar trusses and thin steel sheeting on the soffit acting as the permanent formwork. Researchers such as Wang *et al*. (2016) reported that the casting of concrete onto the steel sheeting and bar trusses significantly improved the strength and rigidity of supporting columns under seismic loading.

The use of lightweight high-strength material can reduce the self-weight of a structural system and increase the structural span. However, such structures may become too slender with low natural frequencies that would be close to the frequency range due to human activity (Nguyen *et al*. 2012, Peng *et al*. 2015, Votsis *et al*. 2017, Wang and Chen 2017). Previous studies related to floor serviceability (Devin and Fanning 2019, Ferreira and Simoes 2019) also indicated that floor vibration intensified with an increasing slab span. Only limited work has been carried out to this date on the vibration response of the composite steel-bar truss slab with steel girder (Liu *et al*. 2019a) and further studies are thus warranted to better understand the vibration issues for such composite floor under human excitations, especially the large-span floor having a low damping. Although floor vibration generally does not affect structural safety, it may cause psychological fear and discomfort to people working or living inside.

Previous studies on building vibration serviceability include wood floors (Dolan *et al*. 1999), RC floors (Zhou *et al*. 2016a), footbridges (Demartino *et al*. 2018, Qin *et al*. 2019, Votsis *et al*. 2017), stairs (Brad Davis and Avci 2015), prestressed concrete truss girder (Cao *et al*. 2018), cold-formed steel floor (Xu *et al*. 2018) and cross-laminated-timber (Edskar and Lidelow 2019, Ussher *et al*. 2017), culminating the vibration serviceability criteria specified in ISO 2631-2 (2003), ATC (Allen *et al*. 1999), BS 6472-1 (2008), and AISC design #11 (Murray *et al*. 2016). Nevertheless, vibration research on the composite steel-bar

*Corresponding author, Ph.D.
E-mail: liangcao@cqu.edu.cn
[a] Professor

ISSN: 1225-4568 (Print), 1598-6217 (Online)

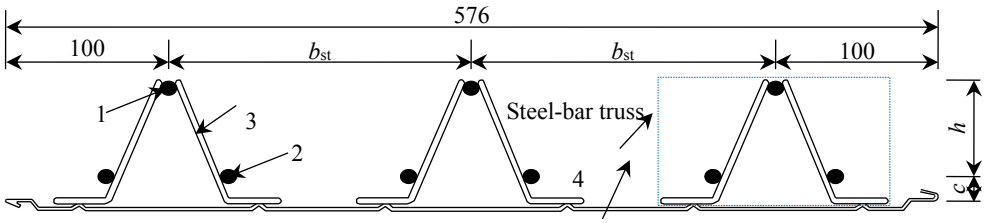

1: Top bar; 2: Bottom bar; 3: Web bar; 4: Baseplate
b_{st}: Distance between the adjacent steel-bar truss; c: Concrete cover thickness; h: Height of steel bar truss

(a) Cross section of steel-bar truss slab

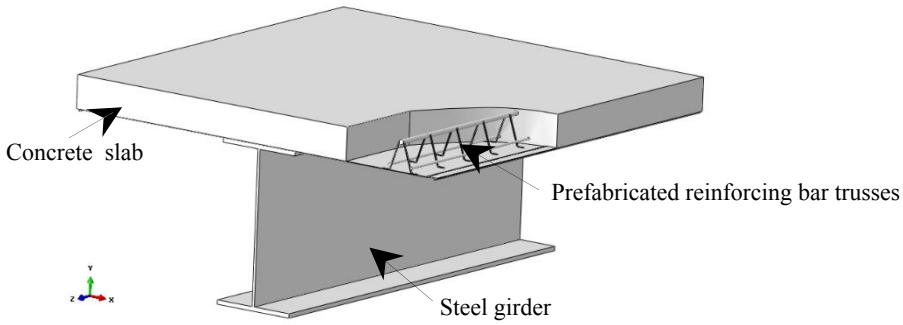

(b) Composite steel-bar truss slab (CSTS) with steel girder

Fig. 1 Diagrams showing the composite steel-bar truss slab with steel girder (unit: mm)

truss slab with steel girder, especially under impulse excitation, is rather limited and requires a further study.

This article discusses the vibration serviceability of composite steel-bar truss slab with steel girder based on the field test. Specifically, the impact tests of heel-drop and jumping were conducted to capture the composite floor's natural frequency and damping ratio, followed by the discussion of the distribution of peak accelerations. Walking and running tests were also performed to capture the vertical acceleration responses, and discuss the human-structure interaction. The objectives of this research are summarized as follows:

- To analyze the acceleration-time relationship under impact excitation (heel-drop and jumping), and then to ascertain the modal parameters and distribution of peak acceleration;
- To analyze the acceleration-time relationship under steady-state motion (walking and running) and evaluate the vibration serviceability of the composite floor;
- To compare the modal parameters obtained from the walking and running vibrations and to verify the human-structure interaction;
- To propose the crest factor β_{rp} for calculating the root-mean-square (RMS) acceleration.

2. Description of prototype floor and accelerometer layout

In-situ test is a practical way to study the vibration performance of the composite steel-bar truss slab (CSTS) with steel girder under human daily activities and to determine its dynamic properties. The investigated CSTS with steel girder was intended to be used in teachers' office.

Table 1 Thickness and material specification for the steel-bar truss slab

Thickness (mm)	c (mm)	Top bar	Bottom bar	Web bar
120	15	C10	C8	A4.5

Table 2 Detailed cross sections and yield strength for the H-shaped steel girders

Steel girder number	Cross section (mm)	Yield strength (MPa)
B01	HN175×90×5×8	345
B02	H500×120×8×10	
B03	H500×150×8×12	
B04	H500×200×10×16	
B05	H600×240×10×20	

The structural arrangement the composite floor is shown in Fig. 2. The thickness and material specification for the steel-bar truss slab are listed in Table 1, and the detailed cross sections and yield strength for H-shaped steel girders are indicated in Table 2. The elasticity modulus of concrete is 3.00×10^4MPa.

Fig. 2 shows the schematic accelerometer locations along with a coordinate system used to obtain the dynamic characteristics and vertical acceleration response of the composite floor, where A_{ij} (i=1-7, j=1-7) represents the jth accelerometer location for the ith test. From the figure, it is known that 50 accelerometers would be needed for one-off measurement. However, the monitoring system used in this study consists of only nine accelerometers ranging ±5g maximum (g being the gravitational acceleration) and a data acquisition system. To overcome the problem, the accelerometers were utilized seven times and the

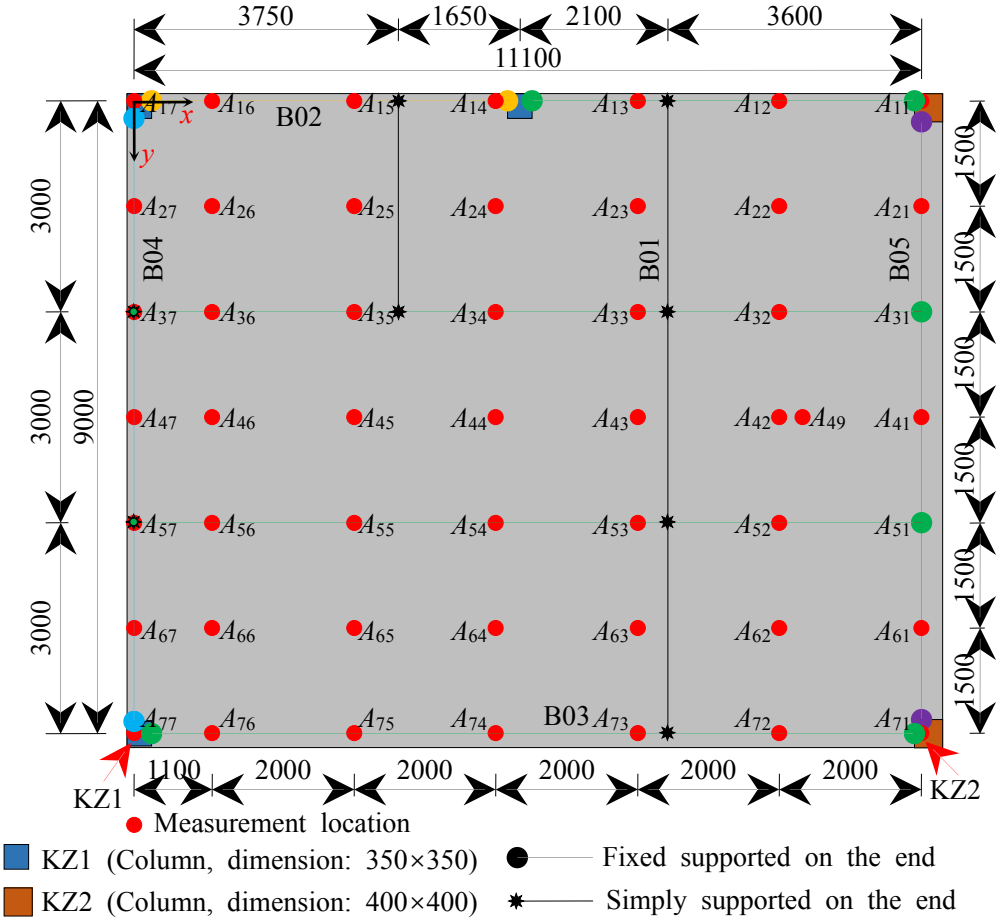

Fig. 2 The structural arrangement of composite floor and layout of accelerometers (unit: mm)

(a) Heel-drop test

(b) Jumping test

Fig. 3 The impulse excitations (unit: mm)

measurement points A_{44} and A_{49} were selected as the stationary location at all time. For example, after the first measurement, the accelerometers were moved from A_{1j} to A_{2j} (j=1-7). The data acquisition system was used to sample all the results collected from these accelerometers at 1000Hz. Before each formal test procedure, a preloading was performed to determine an appropriate acceleration range for recording the acceleration response.

To evaluate the vibration performance of the composite floor due to human activities, a series of field tests were conducted, including impulsive excitation (heel-drop and jumping) and steady-state excitation (walking and running).

3. Impulse excitation

To determine the vibration performance of the composite floor due to the impulse excitation, heel-drop (Fig. 3(a)) and jumping (Fig. 3(b)) tests were conducted. The impact tests were carried out at the successive locations of A_{i4} (i=1, 2, 3, 5, 6,) and A_{49} by two persons with different masses, and the weight of the two persons are 50kg (N_{m1}) and 74kg (N_{m2}), respectively. The testers performed three times at each excitation point to reduce the randomness.

The heel-drop impact is composed of a series of human movements as suggested by the AISC Design Guide #11 (Murray *et al.* 2016). In performing a heel-drop test, the person lifted his heels approximately 80mm off the floor, forcefully impacted the slab with his own weight with both

heels, while carefully avoided multiple strikes, bouncing, or rocking.

The jumping test was conducted by a person in such way: bend both knees, push against the ground with both feet, jump quickly into the air, and drop down to the floor.

The accelerations at each measuring point were measured from the impact tests. The typical acceleration-time response are shown in Fig. 4. The acceleration signals were transformed to frequency response by the fast Fourier transform, and the power spectra corresponding with Fig. 4 are shown in Fig. 5, which indicate that the first peak acceleration occurs at the fundamental natural frequency f_1 of 8.3Hz. This f_1 value implies that the composite floor is relatively flexible compared to others in which f_1 of 10Hz is usually recommended for practical use (Smith *et al*. 2009).

Damping generally implies the dissipation of energy. It reduces the floor vibration and eventually ends the oscillation. Damping is another important design consideration. Based on the acceleration response data collected from the heel-drop and jumping tests, the damping ratio ξ for lightly damped systems can be determined from (Chopra 1995)

$$\xi = \frac{1}{2\pi j} \ln \frac{a_i}{a_{i+j}} \tag{1}$$

where a_i and a_{i+j} are the ith and $(i+j)$th peak accelerations, respectively. In this study, a_1 and a_7 were used to estimate the damping ratio. The vibration signals collected from the accelerations at loading point A_{i4} (i=1-6) and A_{49} were adopted to identify the damping ratio. Table 3 and Table 4 summarizes the damping ratio determined by heel-drop and jumping, respectively. ξ ratios range from 1.16% to 3.78% for the heel-drop tests and from 1.64% to 4.73% for the jumping tests. And it shows that the damping ratio of the composite floor is not a constant. The main reason for the phenomenon is that the human-structure interaction (Liu *et al*. 2020) is induced during an impulse excitation on composite floors (Gaspar *et al*. 2019), and the interaction strength is related to load magnitude, position and so on (Zhou *et al*. 2016b). The average damping ratios conduced from heel-drop and jumping are 2.47% and 2.49%, repressively. For the structural design, ξ value being 2.47% is proposed.

The peak acceleration measured at each incentive point A_{i4} (i=1-6) and A_{49} due to heel-drop and jumping by N_{m1} and N_{m2} on the composite floor are listed in Table 5 and Table 6, respectively. The maximum peak accelerations at each incentive point due to heel-drop and jumping are 71.4×10^{-2}m/s^2 (N_{m1}, A_{44}) and 31.3×10^{-1}m/s^2 (N_{m1}, A_{64}), respectively. As indicated in Table 5 to Table 6, the average peak acceleration at A_{44} is slightly larger than that at other loading points. So, the vicinity of incentive points A_{44} are more unfavorable incentive place for the composite floor vibration.

The ratio α_{hj} of the average peak acceleration at each loading point induced by jumping and heel-drop is listed in Table 7. The range of value of ratio α_{hj} is 1.89 to 4.76, which is similar to the conclusion on the long-span pre-stressed concrete floor (Cao *et al*. 2018). The average value being 2.86 is proposed.

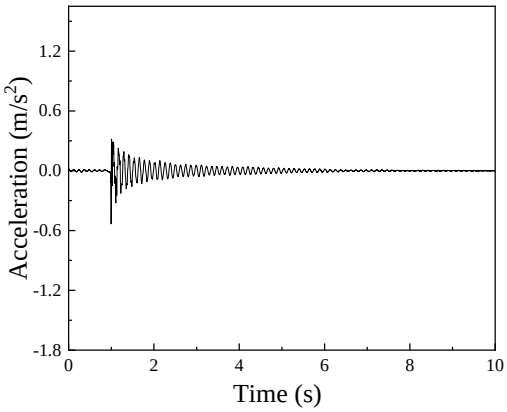

(a) Heel-drop

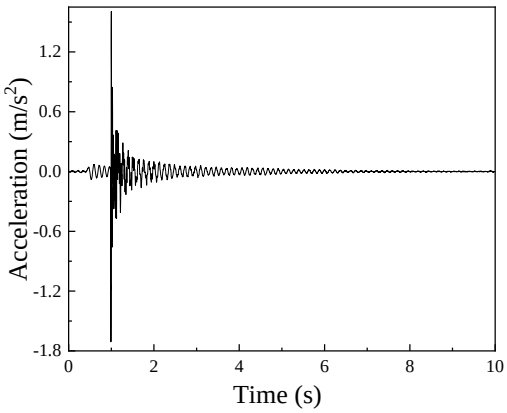

(b) Jumping

Fig. 4 Typical acceleration-time response

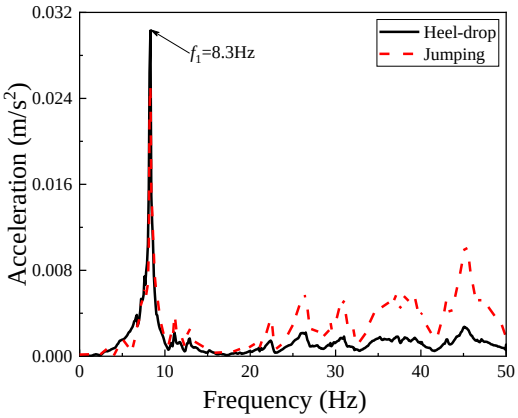

Fig. 5 The corresponding power spectrum of the composite floor

Table 3 The damping ratio conduced from heel-drop (%)

Loading point	N_{m1}			N_{m2}		
	1st	2nd	3rd	1st	2nd	3rd
A_{14}	1.42	1.16	1.16	3.04	2.17	3.13
A_{24}	2.48	2.43	2.54	2.20	2.33	1.99
A_{34}	2.44	2.33	2.69	2.35	2.50	2.48
A_{44}	2.71	2.32	2.61	2.51	2.31	2.41
A_{54}	2.13	1.81	1.68	3.78	3.69	2.11
A_{64}	2.32	1.94	2.02	3.37	3.45	3.25
A_{49}	2.56	2.12	2.25	3.41	3.07	2.94

Table 4 The damping ratio conduced from jumping (%)

Loading point	N_{m1}			N_{m2}		
	1st	2nd	3rd	1st	2nd	3rd
A_{14}	1.66	2.67	1.64	2.37	2.34	2.15
A_{24}	2.62	1.10	2.83	2.64	1.97	2.45
A_{34}	2.09	2.08	1.98	1.77	2.04	1.97
A_{44}	2.72	2.04	2.38	2.05	2.65	2.00
A_{54}	3.03	3.52	2.65	2.24	2.98	2.80
A_{64}	2.83	2.65	3.11	4.73	3.87	3.01
A_{49}	2.36	2.14	2.59	2.62	2.27	2.82

Table 5 The peak acceleration at each incentive point due to heel-drop tests ($\times 10^{-2}$m/s^2)

		A_{14}	A_{24}	A_{34}	A_{44}	A_{54}	A_{64}	A_{49}
N_{m1}	1st	59.2	53.2	44.9	61.8	47.8	45.0	65.7
	2nd	47.7	51.5	30.9	76.7	59.5	43.4	35.5
	3rd	31.2	44.1	42.5	57.1	42.1	43.7	56.5
	Average	46.0	49.6	39.4	65.2	49.8	44.0	52.6
N_{m2}	1st	54.4	67.2	30.9	56.2	48.4	57.7	40.0
	2nd	49.1	68.2	35.6	50.9	47.0	55.5	32.4
	3rd	41.4	55.8	35.4	34.2	31.4	65.7	35.2
	Average	48.3	63.7	34.0	47.1	42.3	59.6	35.9

Table 6 The peak acceleration at each incentive point due to jumping tests ($\times 10^{-2}$m/s^2)

		A_{14}	A_{24}	A_{34}	A_{44}	A_{54}	A_{64}	A_{49}
N_{m1}	1st	75.8	140.1	161.4	169.1	129.2	313.0	188.6
	2nd	131.7	157.3	87.8	116.5	94.8	109.6	120.3
	3rd	71.1	115.8	53.1	174.5	57.6	164.8	125.3
	Average	92.9	137.7	100.8	153.4	93.9	195.8	144.7
N_{m2}	1st	91.7	91.3	162.8	187.6	83.9	115.4	218.0
	2nd	111.6	264.7	121.9	171.0	72.2	271.1	128.8
	3rd	152.7	167.4	82.0	73.6	89.2	94.9	165.7
	Average	118.7	174.5	122.2	144.1	81.8	160.5	170.8

Table 7 Values of the ratios α_{hj}

	Loading point							Average
	A_{14}	A_{24}	A_{34}	A_{44}	A_{54}	A_{64}	A_{49}	
N_{m1}	2.02	2.78	2.56	2.35	1.89	4.45	2.75	2.86
N_{m2}	2.46	2.74	3.59	3.06	1.93	2.69	4.76	

The ratios of acceleration amplitudes at locations A_{4j} (j=1-7) to that at location A_{44} are shown in Fig. 6. From the figures, the boundary condition of the composite floor should be elastic bearing, which is inconsistent with the long-span pre-stressed concrete floor (Zhou *et al*. 2016a); the ratio ranges from 0 and 1 with the maximum value occurring at loading points A_{i4} (i=1-6); the intensity, the location of impact excitation and steel girder have a significant influence on the rate of acceleration decay.

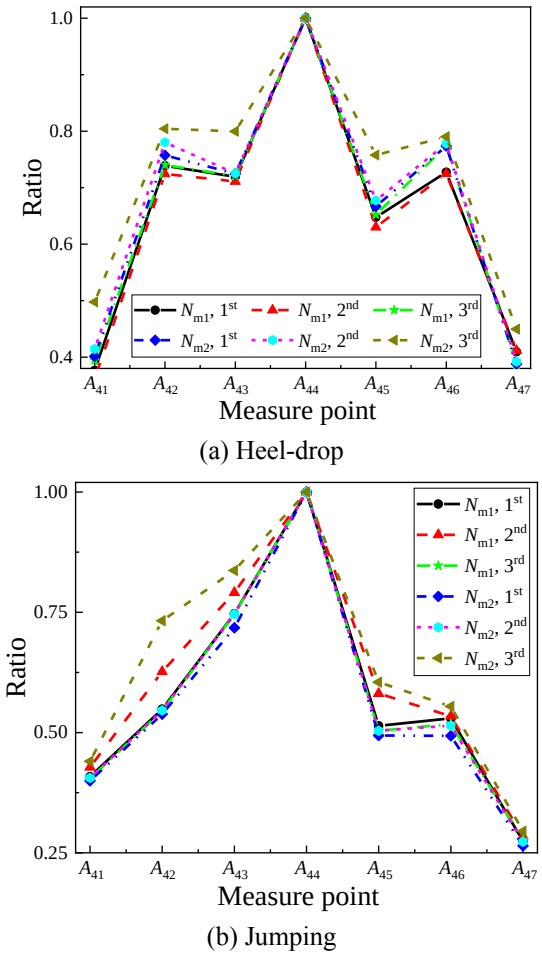

(a) Heel-drop

(b) Jumping

Fig. 6 Average ratios of the acceleration amplitudes between A_{4j} (j=1-7) and A_{44}

4. Boundary conditions

Both numerical and theoretical method were used to determine a reasonable boundary condition for the composite floor. In the numerical simulation, the entire structural system was modeled, in which C3D20 element (20-node quadratic brick) available in ABAQUS program were used and the total number of element was 90518. In the theoretical analysis, the composite floor was idealized as an orthotropic plate, where the fundamental natural frequency f_1 can be determined by the Rayleigh principle (Timoshenko and Woinowsky-Krieger 1959)

$$f_1 = \frac{1}{2\pi}\frac{\alpha_0}{b^2}\sqrt{\frac{g}{q_0}}\sqrt{\alpha_1\frac{D_1}{C^4}+\alpha_2 D_2+\alpha_3\frac{D_3}{C^2}} \quad (1)$$

where C=a/b with a=beam span and b= plate width; D_1 and D_2 are the plate stiffnesses in x and y directions, respectively; D_3 is the combined rigidity; q_0 is the weight per unit area of the plate; and α_0, α_1, α_2, α_3 are the coefficients depending on the boundary condition (Table 8). It should be noted that the boundary conditions listed in Table 8 are in accordance with the convention defined in Fig. 7 and that the vibration mode functions for boundary conditions "CC", "SS" and "SC" are described in Table 9.

Table 8 α_0, α_1, α_2, and α_3 coefficients

Boundary condition	α_0	α_1	α_2	α_3
CCCC	22.45	1.00	1.00	0.571
SSSS	19.72	0.25	0.25	0.500
CSCS	11.39	4.00	0.75	2.00
SCSS	13.96	41/32	0.5	1.25

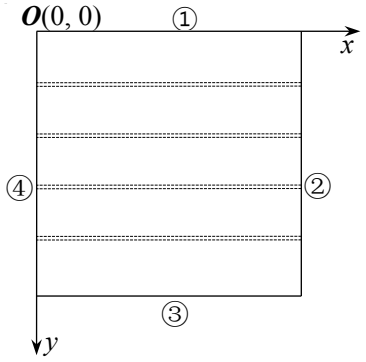

(a) Boundary symbol

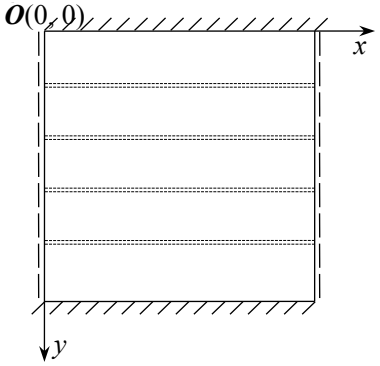

(b) CSCS

Notes: 1. S: simply supported; C: clamped.
2. For example, SCCC represents clamped on edges ①, ③ and simply supported on edges ②, ④.

Fig. 7 The naming conventions on the boundary condition of the composite floor

Table 9 Vibration mode functions for boundary conditions "CC", "SS" and "SC"

Boundary condition	Vibration mode function
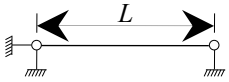	$\sin\frac{\pi x}{L}$
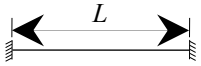	$\cos\frac{2\pi x}{L}-1$
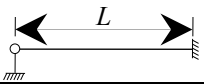	$\cos\frac{3\pi x}{2L}-\cos\frac{\pi x}{2L}$

According to the literatures (Smith *et al*. 2009, Timoshenko and Woinowsky-Krieger 1959) and Fig. 2, the coefficients D_1, D_2, D_3 and q_0 in Eq. (1) were determined as 6.72×10^6N·m, 6.97×10^7N·m, 6.84×10^6N·m and 3082N/m^2, respectively. Table 10 lists the fundamental natural

Table 10 The analytical and numerical fundamental natural frequencies under different boundary conditions and their errors with the measured value

Boundary condition	Method	f_1 (Hz)	Error (%)
CCCC	Theory	7.40	10.84
	FE	7.24	12.77
SSSS	Theory	15.61	88.07
	FE	12.98	56.39
CSCS	Theory	9.65	16.27
	FE	11.83	42.53
SCSS	Theory	8.37	0.84
	FE	8.32	0.24

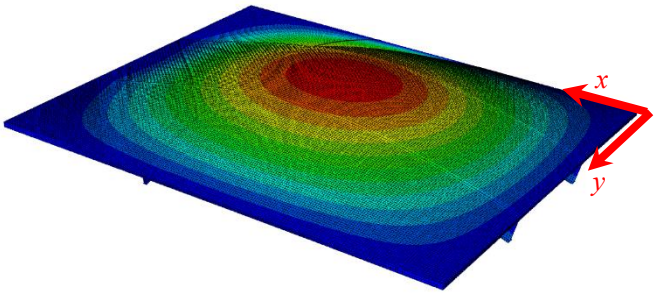

Fig. 8 The first mode shape of composite floor with "SCSS" edge (3D model using ABAQUS)

frequency obtained analytically and numerically under different boundary conditions and the errors with the measured value. Considering the beam-slab stiffness ratio, wall condition, and the effect of adjacent structure (Zhou *et al*. 2017), the boundary condition of "CCCC", "SSSS", "CSCS" or "SCSS" was assumed first for the composite floor. The mode shape of the composite floor with "SCSS" edges are shown in Fig. 8. As noted, under the boundary conditions "CCCC", "SSSS" or "CSCS" the error from either the analytical or the finite element method is quite high. While, under the boundary condition "SCSS" the error is relatively small and both methods yield virtually the same results. Consequently, the boundary condition "SCSS" is deemed more comparable substitutive in performing a theoretical and numerical vibration analyses on human-structure interaction for the investigated composite floor.

5. Steady-state motion

Human-induced vibration serviceability issues could be very complex, involving the magnitude of motion, surrounding environment, and human's perceptibility. A continuous steady-state motion may cause an annoying vibration. So, a series of walking and running tests (single excitation) were performed to estimate the vertical acceleration response and modal parameters of the composite floor. Starting from A_{i1} (i=1-7), each tester walked or run along the following routes repeated for a duration of 5 minutes: $A_{i1}\rightarrow A_{i4}\rightarrow A_{i7}\rightarrow A_{i4}\rightarrow A_{i1}\rightarrow\ldots$. The real frequencies of walking, and running in the daily life are adopted. To obtain the fundamental frequencies for these

Table 11 The walking frequencies along each route (steps/s)

	Route $A_{i1}\rightarrow A_{i4}\rightarrow A_{i7}\rightarrow A_{i4}\rightarrow A_{i1}\rightarrow\ldots$						
	i=1	i=2	i=3	i=4	i=5	i=6	i=7
N_{m1}	1.76	1.68	1.68	1.62	1.66	1.81	1.60
N_{m2}	1.78	1.78	1.79	1.70	1.70	1.77	1.71

Table 12 The running frequencies along each route (steps/s)

	Route $A_{i1}\rightarrow A_{i4}\rightarrow A_{i7}\rightarrow A_{i4}\rightarrow A_{i1}\rightarrow\ldots$						
	i=1	i=2	i=3	i=4	i=5	i=6	i=7
N_{m1}	2.88	2.79	2.90	2.78	2.85	2.81	2.82
N_{m2}	2.39	2.41	2.32	2.35	2.43	2.34	2.35

Table 13 The peak and RMS accelerations at each measuring point due to walking excitation ($\times10^{-3}$m/s^2, N_{m1})

i		Measure points						
		A_{i1}	A_{i2}	A_{i3}	A_{i4}	A_{i5}	A_{i6}	A_{i7}
1	Peak	15.1	30.6	35.3	33.3	36.5	19.1	7.0
	RMS	2.0	4.8	8.7	10.6	7.3	3.5	1.6
2	Peak	18.5	38.9	34.6	41.7	35.4	34.6	16.3
	RMS	4.6	9.2	14.5	17.5	13.2	7.7	3.0
3	Peak	16.9	35.0	44.4	45.0	41.1	31.4	14.3
	RMS	3.3	14.5	21.4	25.7	20.0	12.4	5.1
4	Peak	16.9	35.1	46.7	42.3	42.4	36.8	22.0
	RMS	2.7	12.8	17.4	19.9	15.9	10.9	5.4
5	Peak	17.3	34.0	38.0	42.6	37.3	24.2	17.2
	RMS	2.3	9.1	12.3	14.4	11.6	7.1	4.0
6	Peak	15.5	49.8	46.6	60.8	38.4	41.3	16.9
	RMS	2.2	11.4	11.7	11.1	8.7	5.8	2.6
7	Peak	14.7	52.3	44.7	16.1	24.7	18.2	8.9
	RMS	2.0	6.9	5.9	1.7	4.0	3.7	1.5

loads, the progress of experimental tests is recorded using a video device. Based on the video data recorded from persons N_{m1} and N_{m2}, the fundamental frequencies of walking and running are listed in Table 11 and Table 12, respectively.

5.1 Acceleration response

The response of the composite floor was evaluated in terms of peak and RMS accelerations. Although the peak acceleration is the highest acceleration resulting from an excitation, it gives no indication as to the duration of time that the system is subjected to this level of acceleration. In contrast, the RMS acceleration represents the average measurement of an acceleration-time history, as expressed by (Davis *et al*. 2014, Sa *et al*. 2017)

$$a_{\mathrm{rms}}(t)=\sqrt{\frac{1}{N}\sum_{i=1}^{N}a_i^2(t)} \tag{2}$$

where $a_{\mathrm{rms}}(t)$ is the rolling RMS acceleration at time t; N is the number of acceleration data points measured between t-1 and t+1; and $a_i(t)$ is the ith acceleration data point.

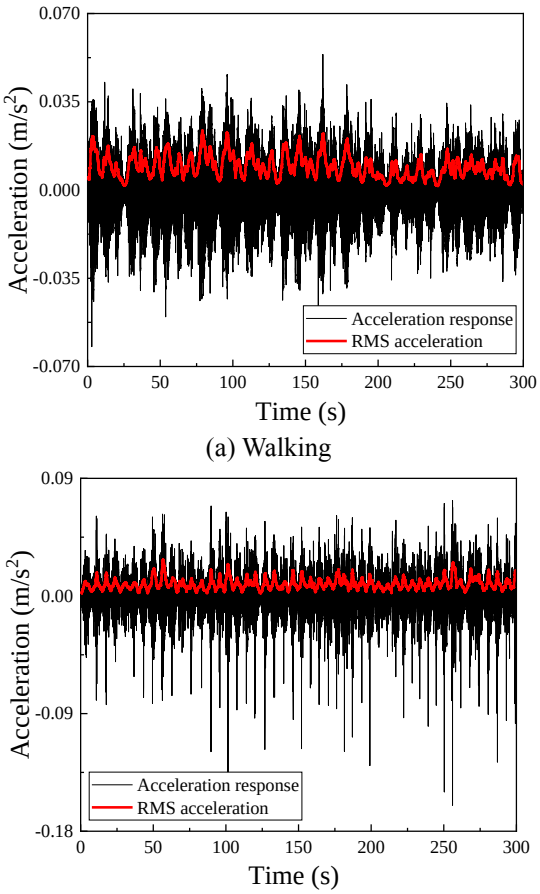

Fig. 9 The acceleration response of the composite floor due to walking and running excitation

Table 14 The peak and RMS accelerations at each measuring point due to walking excitation ($\times10^{-3}$m/s^2, N_{m2})

i		Measure points						
		A_{i1}	A_{i2}	A_{i3}	A_{i4}	A_{i5}	A_{i6}	A_{i7}
1	Peak	16.0	27.8	31.0	39.4	31.1	35.8	10.3
	RMS	2.3	5.0	6.8	7.9	6.2	4.8	2.0
2	Peak	51.6	80.2	66.2	61.4	59.2	96.5	33.9
	RMS	6.6	12.9	11.1	13.2	10.7	13.9	4.9
3	Peak	22.9	62.6	62.6	43.3	46.5	52.9	27.6
	RMS	4.6	11.7	15.8	17.8	14.4	11.2	6.2
4	Peak	25.7	58.9	62.0	62.1	48.8	57.8	28.9
	RMS	4.0	15.7	20.0	23.6	18.7	14.8	7.5
5	Peak	20.2	33.5	35.0	36.0	33.1	35.5	24.2
	RMS	3.0	10.0	12.4	14.7	12.4	8.8	5.6
6	Peak	12.5	39.2	35.9	53.3	56.6	81.0	27.2
	RMS	2.4	8.1	8.6	7.7	9.1	11.1	4.3
7	Peak	8.8	22.6	15.2	7.8	27.2	25.8	9.6
	RMS	2.1	4.3	3.4	1.8	4.7	4.1	1.7

The peak and RMS accelerations (typical example shown in Fig. 9) of the composite floor due to the walking and running excitations along the various routes are listed in

Table 15 The peak and RMS accelerations at each measuring point due to running excitation ($\times 10^{-2}$m/s^2, N_{m1})

	i	Measure points						
		A_{i1}	A_{i2}	A_{i3}	A_{i4}	A_{i5}	A_{i6}	A_{i7}
1	Peak	2.7	15.3	16.2	13.1	10.4	7.9	1.6
	RMS	0.4	1.9	3.1	3.4	2.4	1.3	0.3
2	Peak	9.8	17.1	16.7	18.2	15.9	18.2	7.1
	RMS	1.6	3.3	3.5	3.7	3.1	3.5	1.1
3	Peak	6.3	12.4	13.5	14.0	14.0	11.9	6.1
	RMS	0.9	3.3	4.5	5.2	4.3	3.0	1.2
4	Peak	8.5	18.4	19.9	17.6	14.7	16.1	7.9
	RMS	1.1	4.0	4.3	3.8	3.5	3.4	1.8
5	Peak	7.7	14.3	14.8	21.4	15.6	10.5	6.1
	RMS	0.9	2.7	3.0	3.0	2.5	2.1	1.4
6	Peak	5.1	19.1	19.0	26.6	19.3	24.8	8.3
	RMS	0.7	4.2	4.2	4.4	4.0	3.5	1.2
7	Peak	3.3	14.4	11.6	2.8	12.1	11.8	1.8
	RMS	0.5	2.1	1.7	0.5	2.1	1.7	0.3

Table 16 The peak and RMS accelerations at each measuring point due to running excitation ($\times 10^{-2}$m/s^2, N_{m2})

	i	Measure points						
		A_{i1}	A_{i2}	A_{i3}	A_{i4}	A_{i5}	A_{i6}	A_{i7}
1	Peak	3.4	9.9	7.4	7.9	7.8	6.5	1.9
	RMS	0.4	1.0	1.3	1.1	1.0	1.0	0.3
2	Peak	11.2	18.5	14.2	14.4	12.8	18.7	6.7
	RMS	1.4	2.7	1.9	2.6	2.0	2.8	1.0
3	Peak	7.2	8.2	7.5	8.2	9.0	10.3	6.8
	RMS	0.9	2.0	2.2	2.0	1.9	2.0	1.1
4	Peak	4.5	15.4	14.1	16.0	15.6	18.5	8.3
	RMS	0.7	2.6	3.0	2.8	2.6	2.5	1.4
5	Peak	4.4	7.3	7.0	6.0	8.5	10.7	7.4
	RMS	0.6	2.3	2.2	1.4	1.6	1.8	1.2
6	Peak	2.0	13.6	14.6	18.5	17.3	24.2	9.4
	RMS	0.5	1.8	1.6	2.1	2.0	2.7	1.0
7	Peak	2.0	4.3	2.9	1.4	5.9	5.2	1.3
	RMS	0.3	0.6	0.5	0.2	0.8	0.7	0.2

Table 13 to Table 16, respectively. From these tables, the maximum peak and RMS acceleration are found to be approximately equal to 96.5×10^{-3}m/s^2(=0.98%g) and 25.7×10^{-3}m/s^2(=0.26%g) for walking excitation, and 26.6×10^{-2}m/s^2(=2.71%g) and 5.2×10^{-2}m/s^2(=0.53%g) for running excitation, respectively. All the RMS accelerations indicated in Table 13, Table 14, Table 15, and Table 16 are below the vibration acceptability limit of 1.5%g specified in the AISC (Murray *et al*. 2016).

5.2 Crest factor β_{rp}

The RMS acceleration is usually used to assess the vibration serviceability (Murray *et al*. 2016). The determination of RMS accelerations involves a tedious calculation process which is inconvenient to engineers. This study proposes a crest factor β_{rp}, as describing by Eq. (3), to facilitate the calculation of RMS accelerations.

$$\beta_{rp} = \frac{a_{Peak}}{a_{rms}} \tag{3}$$

Table 17 β_{rp} factors corresponding to the walking excitation on the composite floor

Tester	i	Measure points						
		A_{i1}	A_{i2}	A_{i3}	A_{i4}	A_{i5}	A_{i6}	A_{i7}
N_{m1}	1	7.55	6.38	4.06	3.14	5.00	5.46	4.38
	2	4.02	4.23	2.39	2.38	2.68	4.49	5.43
	3	5.12	2.41	2.07	1.75	2.06	2.53	2.80
	4	6.26	2.74	2.68	2.13	2.67	3.38	4.07
	5	7.52	3.74	3.09	2.96	3.22	3.41	4.30
	6	7.05	4.37	3.98	5.48	4.41	7.12	6.50
	7	7.35	7.58	7.58	9.47	6.18	4.92	5.93
N_{m2}	1	6.96	5.56	4.56	4.99	5.02	7.46	5.15
	2	7.82	6.22	5.96	4.65	5.53	6.94	6.92
	3	4.98	5.35	3.96	2.43	3.23	4.72	4.45
	4	6.43	3.75	3.10	2.63	2.61	3.91	3.85
	5	6.73	3.35	2.82	2.45	2.67	4.03	4.32
	6	5.21	4.84	4.17	6.92	6.22	7.30	6.33
	7	4.19	5.26	4.47	4.33	5.79	6.29	5.65

Table 18 β_{rp} factors corresponding to the running excitation on the composite floor

Tester	i	Measure points						
		A_{i1}	A_{i2}	A_{i3}	A_{i4}	A_{i5}	A_{i6}	A_{i7}
N_{m1}	1	6.75	8.05	5.23	3.85	4.33	6.08	5.33
	2	6.13	5.18	4.77	4.92	5.13	5.20	6.45
	3	7.00	3.76	3.00	2.69	3.26	3.97	5.08
	4	7.73	4.60	4.63	4.63	4.20	4.74	4.39
	5	8.56	5.30	4.93	7.13	6.24	5.00	4.36
	6	7.29	4.55	4.52	6.05	4.83	7.09	6.92
	7	6.60	6.86	6.82	5.60	5.76	6.94	6.00
N_{m2}	1	8.50	9.90	5.69	7.18	7.80	6.50	6.33
	2	8.00	6.85	7.47	5.54	6.40	6.68	6.70
	3	8.00	4.10	3.41	4.10	4.74	5.15	6.18
	4	6.43	5.92	4.70	5.71	6.00	7.40	5.93
	5	7.33	3.17	3.18	4.29	5.31	5.94	6.17
	6	4.00	7.56	9.13	8.81	8.65	8.96	9.40
	7	6.67	7.17	5.80	7.00	7.38	7.43	6.50

Table 19 Average β_{rp} factors for different steady-state excitations on the composite floor

Walking	Running
4.72	5.97

Table 20 Modal properties of the composite floor under walking and running excitations

	Modal parameters	Walking	Running
N_{m1}	Frequency (Hz)	8.316	8.301
	Damping ratio (%)	0.9	1.2
N_{m2}	Frequency (Hz)	8.255	8.270
	Damping ratio (%)	0.9	0.8

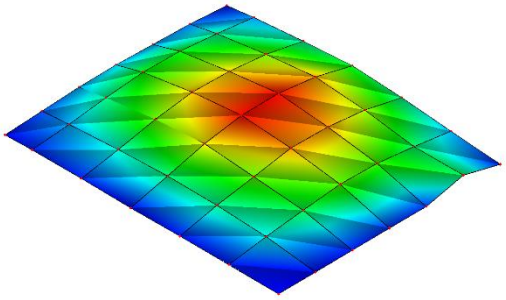

(a) N_{m1}

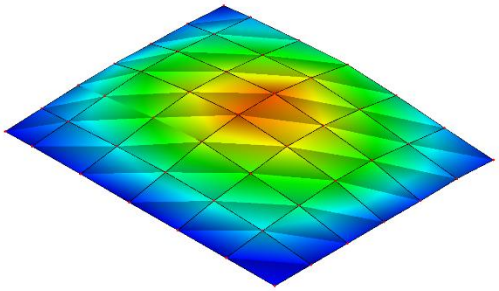

(b) N_{m2}

Fig. 10 The first vertical mode shape of composite floor determined by walking excitation

Based on the Grubbs' criterion contained in GB/T 4883-2008 (2008), individual β_{rp} factors and the average value under a detection level α_{lev} = 0.05 can be obtained, as summarized in Table 17, Table 18 and Table 19. For design convenience and safety, β_{rp} being 4.72 and 5.97 are suggested for walking and running, excitation respectively.

6. Human-structure interaction

The modal parameters (including natural frequency, damping ratio and mode shape) (Arani *et al*. 2017, Liu *et al*. 2019b) of the composite floor can also be determined by the walking and running excitations. The natural frequencies and damping ratios determined by the walking and running excitations are listed in Table 20, and the mode shape of the composite floor determined by walking and running excitation are shown in Fig. 10 and Fig. 11, respectively. Comparisons of the mode shapes along different acceleration point obtained by the walking and running tests are presented in Fig. 12. The table and figure show that the modal parameters determined by the walking and running excitations are not exactly the same. Some significant differences are noted. The main reason for this is that the walk and running behaviour of a person will influence the vibration characteristics of a long span and light-weight floor (Liu *et al*. 2019a, Shahabpoor *et al*. 2016), i.e., having the effect of human-structure interaction. The interaction effect will reduce the damping ratio of the composite floor.

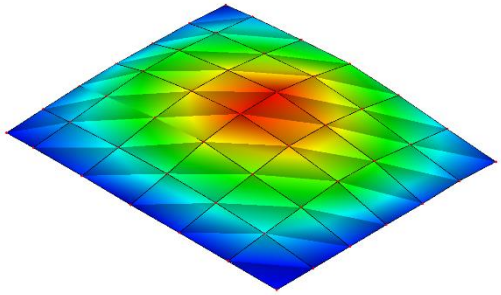

(a) N_{m1}

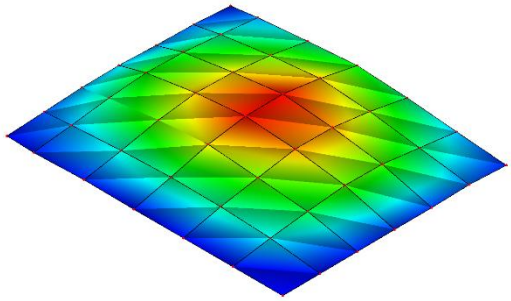

(b) N_{m2}

Fig. 11 The first vertical mode shape of composite floor determined by running excitation

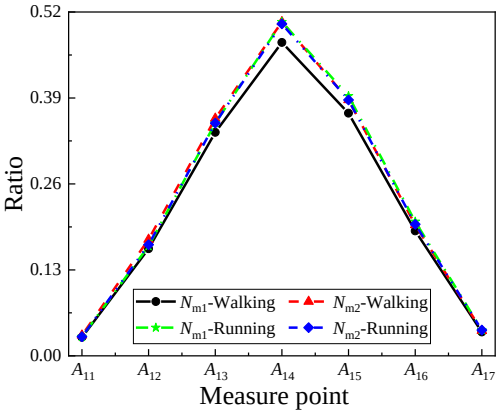

(a) A_{11}-A_{14}-A_{17}

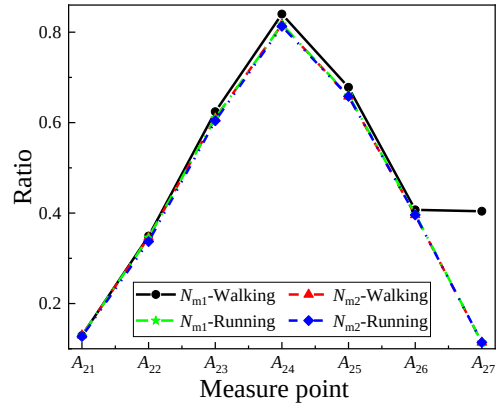

(b) A_{21}-A_{24}-A_{27}

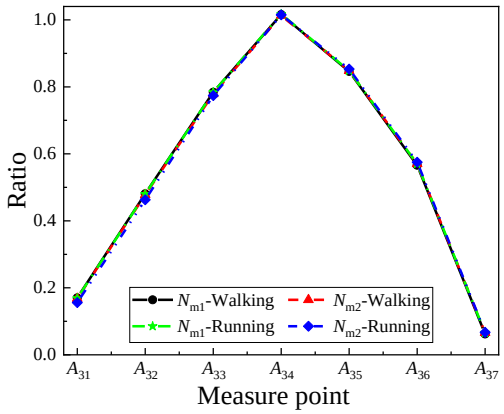

(c) A_{31}-A_{34}-A_{37}

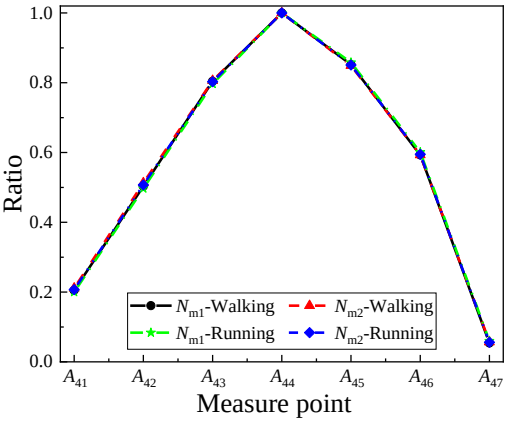

(d) A_{41}-A_{44}-A_{47}

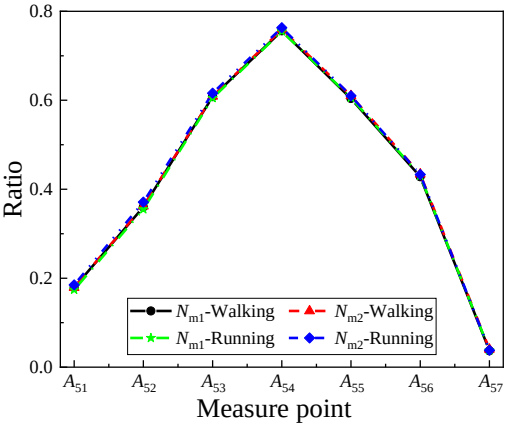

(e) A_{51}-A_{54}-A_{57}

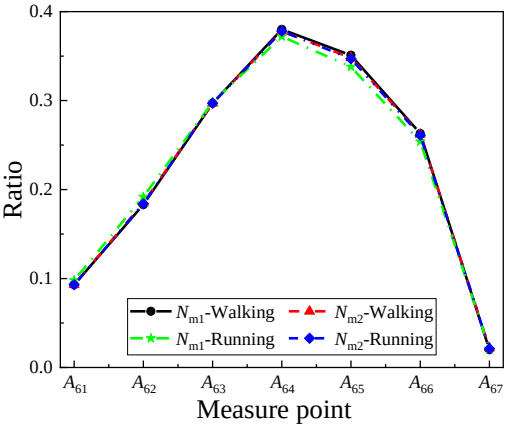

(f) A_{61}-A_{64}-A_{67}

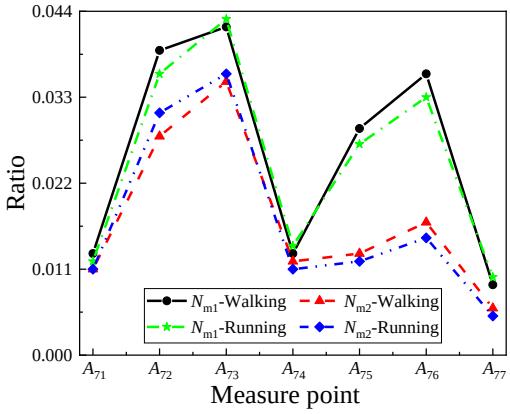

(g) A_{71}-A_{74}-A_{77}

Fig. 12 Comparison of the first vertical mode shapes for the composite floor along different acceleration points

7. Conclusions

A comprehensive research was undertaken to study the vibration serviceability of the composite steel-bar truss slab (CSTS) with steel girder, where the impulse excitation (heel-drop and jumping) and steady-state motion (walking and running) were conducted on-site. Based on the study results, the following primary findings and conclusions are offered:

- The fundamental natural frequency of the composite floor is 8.3Hz, indicating that the composite floor is relatively flexible since the frequency is under the recommended practical value of 10Hz. And avoiding human-induced vibration serviceability problem, the stiffness should be increased.
- The damping ratio for the first mode of the composite floor is 2.42%, all up the AISC suggested limit of 2.00% for bare floors. The damping ratio obtained from walking and running excitations is much lower than that obtained from impulse excitation, and the main reason is the human-structure interaction.
- The fundamental natural frequency of the investigated composite floor obtained from the theoretical or numerical method are very different from the experimental results for the boundary condition “CCCC”, “SSSS”, “CSCS”, while they are relatively close to each other for the boundary condition SCSS. Hence, the boundary condition “SCSS” is recommended for studying the vibration behavior of the investigated composite floor.
- The area near location A_{44} (Fig. 2) is deemed as the unfavorable spot in terms of the composite floor vibration. The maximum peak accelerations at each incentive point due to heel-drop and jumping are 71.4×10^{-2}m/s^2 (N_{m1}, A_{44}) and 31.3×10^{-1}m/s^2 (N_{m1}, A_{64}), respectively.
- The acceleration response induced by jumping excitation is 2.55 times larger than that induced by heel-drop.
- All obtained RMS accelerations due to walking and running excitation appear to satisfy the AISC vibration criterion since the maximum value is 0.53%g.
- For design convenience and safety, the crest factor β_{rp} (ratio of peak to RMS accelerations) can be set at 4.72

and 5.97 for walking and running excitation.

- The comparisons of modal parameters (natural frequency, damping ratio, and mode shape) among the walking and running tests show that the walking and running behavior of a person will influence the vibration characteristics of a long span and light-weight floor, i.e., having the effect of human-structure interaction.
- The interaction effect will reduce the damping ratio of the composite floor.

Acknowledgments

The authors are grateful to the supports provided by the National Natural Science Foundation of China (Grant No. 51908084) and Natural Science Foundation of Chongqing, China (Project No. cstc2019jcyj-bshX0013).

References

Allen D.E., Onysko D.M. and Murray T.M. (1999), ATC design guide 1: minimizing floor vibration. Applied Technology Council, USA.

Arani, A.G., Maraghi, Z.K. and Ferasatmanesh, M. (2017), "Theoretical investigation on vibration frequency of sandwich plate with PFRC core and piezomagnetic face sheets under variable in-plane load", *Struct. Eng. Mech.*, **63**(1), 65-76. https://doi.org/10.12989/sem.2017.63.1.065.

BS 6472-1 (2008), Guide to evaluation of human exposure to vibration in buildings Part 1: Vibration sources other than blasting. British Standards Institution, United Kingdom.

Cao, L., Liu, J.P. and Chen, Y.F. (2018), "Vibration performance of arch prestressed concrete truss girder under impulse excitation", *Eng. Struct.*, **165**, 386-395. https://doi.org/10.1016/j.engstruct.2018.03.050.

Cao, L., Qi, H.T. and Li, J. (2018), "Experimental and numerical studies on the vibration serviceability of fanshaped prestressed concrete floor", *Int. J. Distrib. Sens. N.*, **14**(8), 1550147718795746. ttps://doi.org/10.1177/1550147718795746.

Chopra, A.K. (1995), *Dynamics of Structures Theory and Application to Earthquake Engineering* (2nd Edition), A Simon & Schuster Company, USA.

Devin, A. and Fanning, P.J. (2019), "Non-structural elements and the dynamic response of buildings: A review", *Eng. Struct.*, **187**, 242-250. https://doi.org/10.1016/j.engstruct.2019.02.044.

Davis, B. and Avci, O. (2015), "Simplified vibration serviceability evaluation of slender monumental stairs", *J. Struct. Eng.*, **141**(11), 04015017. https://doi.org/10.1061/(ASCE)ST.1943-541X.0001256.

Davis, B., Liu, D. and Murray, T.M. (2014), "Simplified experimental evaluation of floors subject to walking induced vibration", *J. Perform. Constr. Fac.*, **28**(5), 04014023. https://doi.org/10.1061/(ASCE)CF.1943-5509.0000471.

Demartino, C., Avossa, A.M. and Ricciardelli, F. (2018), "Deterministic and probabilistic serviceability assessment of footbridge vibrations due to a single walker crossing", *Shock Vib.*, **2018**, 1917629. https://doi.org/10.1155/2018/1917629.

Dolan J.D., Murray T.M., Johnson J.R., Runte D. and Shue B.C. (1999), "Preventing annoying wood floor vibrations", *J. Struct. Eng.*, **125**(1), 19-24. https://doi.org/10.1061/(ASCE)0733-9445(1999)125:1(19).

Edskar, I. and Lidelow, H. (2019), "Dynamic properties of cross-laminated timber and timber truss building systems", *Eng. Struct.*, **186**, 525-535. https://doi.org/10.1016/j.engstruct.2019.01.136.

Ferreira, F. and Simoes, L. (2019), "Optimum design of a controlled cable-stayed footbridge subject to a running event using semiactive and passive mass dampers", *J. Perform. Constr. Fac.*, **33**(3), 04019025. https://doi.org/10.1061/(ASCE)CF.1943-5509.0001285.

Gaspar, C., Caetano, E., Moutinho, C. and da Silva, J.G.S. (2019), "Active human-structure interaction during jumping on floors", *Struct. Control Health Monit.*, e2466. https://doi.org/10.1002/stc.2466.

ISO 2631-2 (2003), Mechanical vibration and shock-evaluation of human exposure to whole-body vibration. Part 2: Vibration in buildings (1Hz to 80Hz). International Organization for Standardization, Geneva.

Jimenez-Alonso, J.F., Saez, A., Caetano, E. and Cunha, A. (2014), "Proposal and calibration of an human-structure interation biomechanical model by the resolution of the inverse dynamic problem", *Proceedings of the 9th International Conference on Structural Dynamic*, EURODYN, Porto, Portugal, June.

Jrad, H., Mars, J., Wali M. and Dammak, F. (2018), "An extended finite element method for modeling elastoplastic FGM plate-shell type structures", *Struct. Eng. Mech.*, **68**(3), 299-312. https://doi.org/10.12989/sem.2018.68.3.299.

Liu, J.P., Cao, L. and Chen, Y. F. (2019a), "Vibration performance of composite steel-bar truss slab with steel girder", *Steel Compos. Struct.*, **30**(6), 577-589. https://doi.org/10.12989/scs.2019.30.6.577.

Liu, J.P., Cao, L. and Chen, Y.F. (2019b), "Analytical solution for free vibration of multi-span continuous anisotropic plates by the perturbation method", *Struct. Eng. Mech.*, **69**(3), 283-291. https://doi.org/10.12989/sem.2019.69.3.283.

Liu, J.P., Cao, L. and Chen, Y.F. (2020), "Theoretical analysis of human–structure interaction on steel-concrete composite floors", *J. Eng. Mech.*, 2020, **146**(4): 04020007. https://doi.org/10.1061/(ASCE)EM.1943-7889.0001740.

Mokhtari, A. and Mirdamadi, H.R. (2018), "Study on vibration and stability of an axially translating viscoelastic Timoshenko beam: Non-transforming spectral element analysis", *Appl. Math. Model.*, **56**, 342-358. https://doi.org/10.1016/j.apm.2017.12.007.

Murray, T.M., Allen, D.E., Ungar, E.E. and Davis, D.B. (2016), Vibrations of Steel-Framed Structural Systems Due to Human Activity (2nd Edition), American Institute of Steel Construction, Inc., Chicago, USA.

Nguyen, T.H., Gad, E.F., Wilson, J.L. and Haritos, N. (2012), "Improving a current method for predicting walking-induced floor vibration", *Steel Compos. Struct.*, **13**(2), 139-155. https://doi.org/10.12989/scs.2012.13.2.139.

Peng, Y.X., Chen, J. and Ding, G. (2015), "Walking load model for single footfall trace in three dimensions based on gait experiment", *Struct. Eng. Mech.*, **54**(5), 937-953. https://doi.org/10.12989/sem.2015.54.5.937.

Qin, S.Q., Zhou, Y.L. and Kang, J.T. (2019), "Footbridge serviceability analysis: From system identification to tuned mass damper implementation", KSCE *J. Civ. Eng.*, **23**(2), 754-762. https://doi.org/10.1007/s12205-018-0985-7.

Sa, M.F., Guerreiro, L., Gomes, A.M., Correia, J.R. and Silvestre, N. (2017), "Dynamic behaviour of a GFRP-steel hybrid pedestrian bridge in serviceability conditions. Part 1: Experimental study", *Thin Wall. Struct.*, **117**, 332-342. https://doi.org/10.1016/j.tws.2017.05.013.

Shahabpoor, E., Pavic, A. and Racic, V. (2016), "Identification of mass-spring-damper model of walking humans", *Struct.*, **5**, 233-246. https://doi.org/10.1016/j.istruc.2015.12.001.

Smith, A.L., Hicks, S.J. and Devine, P.J. (2009), *Design of Floors for Vibration*: *A New Approach*, The Steel Construction Institute, Ascot, Berkshire, British.

Timoshenko, S. and Woinowsky-Krieger, S. (1959), *Theory of Plates and Shells*, Mcgraw-Hill College, New York, USA.

Ussher, E., Arjomandi, K., Weckendorf, J. and Smith, I. (2017), "Prediction of motion responses of cross-laminated-timber slabs", *Struct*., **11**, 49-61. https://doi.org/10.1016/j.istruc.2017.04.007.

Votsis, R.A., Stratford, T.J., Chryssanthopoulos, M.K. and Tantele, E.A. (2017), "Dynamic assessment of a FRP suspension footbridge through field testing and finite element modelling", *Steel Compos. Struct*., **23**(2), 205-215. https://doi.org/10.12989/scs.2017.23.2.205.

Wang, A.J. (2017), "Experimental studies into a new type of hybrid outrigger system with metal dampers", *Struct. Eng. Mech*., **64**(2), 183-194. https://doi.org/10.12989/sem.2017.64.2.183.

Wang, J.P. and Chen, J. (2017), "A comparative study on different walking load models", *Struct. Eng. Mech*., **63**(6), 847-856. https://doi.org/10.12989/sem.2017.63.6.000.

Wang, Q.H., Ranzi, G., Wang, Y.Y. and Geng, Y. (2016), "Long-term behaviour of simply-supported steel-bars truss slabs with recycled coarse aggregate", *Constr. Build. Mater*., **116**, 335-346. https://doi.org/10.1016/j.conbuildmat.2016.04.150.

Xu, L., Zhang, S.G. and Yu, C. "Determination of equivalent rigidities of cold-formed steel floor systems for vibration analysis, Part II: evaluation of the fundamental frequency", *Thin Wall Struct*., **132**, 1-15. https://doi.org/10.1016/j.tws.2018.08.002.

Yan, W.Y., and Lu, F.W. (2015), "Structural analysis of the steel-bars truss formwork in construction", *Struct. Eng*., **31**(4), 206-210. https://doi.org/10.15935/j.cnki.jggcs.2015.04.029.

Zhou, X.H., Cao, L., Chen, Y.F., Liu, J.P. and Li, J. (2016a), "Experimental and analytical studies on the vibration serviceability of pre-stressed cable RC truss floor systems", *J. Sound Vib*., **361**, 130-147. https://doi.org/10.1016/j.jsv.2015.10.001.

Zhou, X.H., Li, J. and Liu, J.P. (2016b), "Vibration of prestressed cable RC truss floor system due to human activity", *J. Struct. Eng*., **142**(5), 04015170. http://dx.doi.org/10.1061/(ASCE)ST.1943-541X.0001447.

Zhou, X.H., Liu, J.P., Cao, L. and Li, J. (2017), "Vibration serviceability of pre-stressed concrete floor system under human activity", *Struct. Infrastruct. E*., **13**(8), 967-977. http://dx.doi.org/10.1080/15732479.2016.1229796.

PL